Part I
Powders

Ceramics Science and Technology: Volume3: Synthesis and Processing, First Edition.
Edited by Ralf Riedel and I-Wei Chen

1
Powder Compaction by Dry Pressing

Rainer Oberacker

1.1
Introduction

Powder compaction by dry pressing is industry's preferred and most widely used forming method for ceramic parts. This can be explained by the high efficiency of the process, which has two variants: uniaxial die pressing; and isostatic pressing. Both methods can be automated to a high degree and are used in the mass production of parts such as ceramic cutting tools (via uniaxial pressing) or spark plug insulators (via isostatic pressing). Uniaxial die pressing produces shapes with accurate dimensions in large quantities, in the shortest cycle times. Compared to injection molding, dry pressing requires a relatively small amount of additives ($\sim$2%), and thus allows for less expensive additive removal operations. However, as fine powders lack the flowability required for the process, in general they must be transformed into a free-flowing press granulate, by employing a granulation process. A second problem results from the nonuniform pressure transmission, leading to nonuniform particle arrangements and density variations in the compacts, which is a well-known source of nonuniform grain growth and other sintering defects [1]. This chapter provides a brief but current review of the fundamental aspects of dry pressing, the practice of uniaxial die and isostatic pressing, and the granulation of fine ceramic powders to granulates. Further details can be found in a number of monographs and reference books (e.g. Refs [2–10]).

1.2
Fundamental Aspects of Dry Pressing

The aim of the process is to transform loose powders into a green compact with a desired shape and a maximal overall density. Close geometrical tolerances, minimal variations of density, packing homogeneity, and sufficient strengths and integrity to withstand the stresses occurring during the subsequent handling, debindering and sintering treatment are further properties required of the green compact. These

Ceramics Science and Technology: Volume3: Synthesis and Processing, First Edition.
Edited by Ralf Riedel and I-Wei Chen

properties are determined by the behavior of the powders during the pressing process. The unit operations of this process are filling of the die or mold, compaction of the powder under a particular state of stress and, in the case of uniaxial die pressing, ejection of the green compact from the die.

1.2.1 Die or Mold Filling Behavior of Powders

Free-flowing powders are a precondition for automated pressing operations, and for achieving reproducible filling densities during the filling step. Free-flowing behavior requires particle sizes above a critical diameter d_c, which is explained by force considerations (Figure 1.1) [3]. The friction forces F_f are proportional to the cohesive forces F_a, which result from van der Waals and electrostatic forces or capillary bridges [11]. They scale linearly with the particle diameter. These must be overcome by the inertial force F_i that is proportional to the particle mass, and which scales with the third power of the particle diameter d_p. At high F_f/F_i, the powders become cohesive and do not flow. The tapping density is independent of particle diameter beyond d_c, but decreases with decreasing particle diameter below d_c which, for ceramic powders, is in the range of several tens of microns.

Most ceramic powders are in the micrometer or submicrometer range, and thus are cohesive. Such powders can be made free-flowing by size enlargement via controlled agglomeration (granulation). Ideally, agglomerates of a spherical shape with a homogeneous packing of the primary particles and a defined porosity and agglomerate size distribution should result from the granulation process. Suitable granule diameters range between 20 and 200 μm. Pressing aids such as binders and plasticizers can be easily incorporated into the granules. Ready-to-press granulates provide flowability, but they also prevent dusting and particle intrusion into the gaps between punches and die, which would result in catastrophic tooling wear.

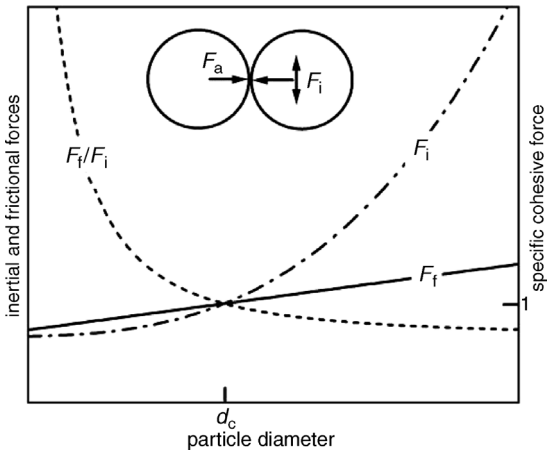

Figure 1.1 Effects of particle diameter on the forces of friction F_f and inertia F_i between particles [3].

1.2.1.1 Particle Packing: A Static View

An important characteristic of the granulates is the packing structure they achieve as they fill the die. A reproducible and sufficiently high apparent packing density is essential for avoiding defects during the subsequent compaction step. Geometrical aspects of particle (granulate) packing have been treated in detail [12] and subsequently reviewed [13]. The models developed in these texts are based on spherical particles with monomodal, bimodal, and polymodal size distributions.

Monosize spheres can, in principle, be arranged in regular three-dimensional (3-D) patterns with a maximal packing density of ~74% for (hexagonal hcp or face-centered fcc) close-packed structures. This can be regarded as an upper limit. The simple cubic structure (sc) exhibits a packing density of ~52%, but is acutely unstable and tends towards the hcp or fcc structure under a mechanical disturbance.

Regular packing arrangements are achieved in practice only over very small domains. Much more of practical relevance are random packings; that is, disordered collections of particles in contact with a maximum density close to 64% for monosized spheres [12–15]. Referred to as random dense packing (RDP) or random close packing (RCP), these are experimentally achieved by pouring uniform balls into a vessel and vibrating this arrangement. The system achieved without vibration is termed random loose packing (RLP), with experimentally observed densities of about 58–60%. Computer simulations [16–18] and advanced characterization methods such as computer tomography [15] have led to a better understanding of such random structures. Random packings would be better referred to as "random jammed states"; jammed packings exist, in theory, over the density range of 53.6 to 63.4%. Depending on the friction coefficient between the particles, in the jammed state only a certain number (Z) of the particle contacts is mechanically loaded. For frictionless particles $Z = 6$, while $Z = 4$ for infinitely rough particles. As illustrated by the phase diagram for jammed matter (Figure 1.2), a packing of monosize spheres with $Z = 5$ can exist only for densities between 59.1 ($D_{RLP}(Z = 5)$) and 63.4 % (D_{RCP}). All states below D_{RCP} tend to increase the density during vibration, until D_{RCP} is reached.

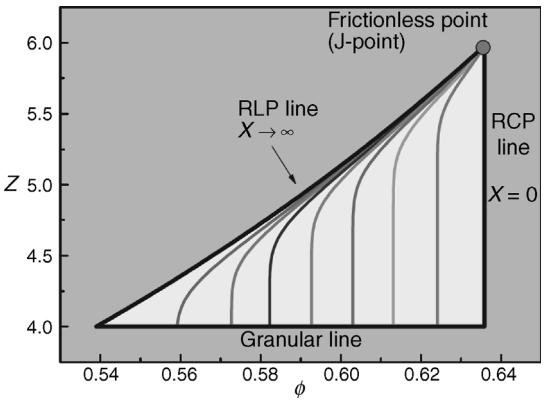

Figure 1.2 Phase diagram of jammed matter [18]. Reprinted with permission from Macmillan Publishers Ltd: [Nature]; © 2008.

Interestingly, the density of random packing of slightly deformed spheres can reach about 70%, significantly more than the D_{RCP} of spheres; for higher aspect ratios, however, the density begins to decrease [14]. The packing density is also enhanced by size-polydispersity. Bimodal spheres pack more densely than uniform spheres, as illustrated in Figure 1.3, where the smaller spheres fill the interstices between random dense-packed larger spheres. The density increases until the interstices are completely occupied, which occurs when the fraction of small spheres reaches about 27% of the total volume of the spheres. If large spheres are placed into a RDP of small spheres, each large sphere increases the local density from $D = D_{RCP}$ to $D = 100\%$, which is true up to 73 vol.% of large spheres. Simple analytical rules of mixture were derived for these filling and replacement operations, assuming an infinite size ratio $(d_L/d_S) \rightarrow \infty$ [12]. Experimental observations for mixtures with finite size ratios follow these upper bounds at lower density levels, as shown schematically in Figure 1.3. Computer simulations for a finite size ratio confirm these correlations [19]. Size ratios $(d_L/d_S) > 7$ are required for a substantial density increase, a fact which can be explained qualitatively by the interstice size of the packing, since small particles have to pass through a critical pore entrance diameter d_e with a dimension of $0.154 \cdot d_L$ for both fcc and hcp packings. This is close to $(d_L/d_S) \approx 7$, where packing enhancement by smaller particles approaches its optimum.

In principle, the interstices between the smaller spheres can be filled by a third population of even smaller particles, and so on. In this way, about 95% and 97% packing density can be achieved in ternary and quaternary mixtures, respectively [13]. However, the required size ratio becomes impractical: ternary mixtures become effective only with size ratios $>10^2$, and quaternary mixtures with size ratios $>10^4$. In practice, the suitable size ratio of industrial granulates is limited to about 10.

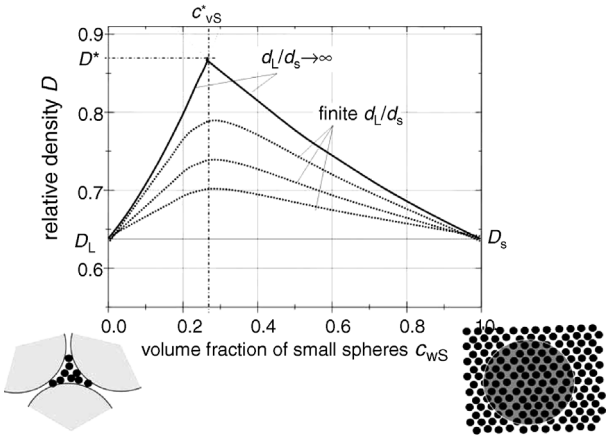

Figure 1.3 Packing density of binary mixtures of spheres according to the analytical solution in Ref. [12].

1.2.1.2 Practical Aspects of Die Filling With Granulates

Practical filling densities are lower than theoretical random packing, as not all particles reach the optimal position during the filling process. In addition, wall effects limit the packing arrangement. Close to the die walls, the packing density is reduced over a distance of 10 to 50 particle diameters, according to monosize sphere experiments, a fact which must be taken into account for components with thin cross-sections. The porosity of the granules also reduces the overall packing density. A hierarchical packing structure is generated when a cavity is filled with such granulates (Figure 1.4). The voids in this packing can be classified as interstices and packing flaws; both types are present at two levels – the level of primary particles and the level of granules.

The filling density D_{fill} of granulates can be calculated as the product of the granule packing structure D_{pack} and the granule density D_{gran} (Eq. (1)):

$$D_{\text{fill}} = D_{\text{pack}} \cdot D_{\text{gran}} \tag{1}$$

Assuming a monosize-sphere RDP of primary particles inside the granules and of the granules ($D_{\text{gran}} = D_{\text{pack}} = 0.64$), a fill density of about 40% would be expected.

The fill density is experimentally characterized by parameters such as apparent density and tap density [20]. The apparent density is determined by filling a standard container through a standard funnel (e.g., Hall flowmeter [21]) with the powder, which is similar to die filling. The tap density is the density of a vertically vibrated powder packing, obtained after being tapped by a standard tapping apparatus until no further densification becomes visible. The ratio of these densities is an index of hindered flow and filling [2]. Apparent densities in the order of 20–35% are typically achieved with spray-dried granulates (see Figure 1.8 below), significantly below the hierarchical random monosize-sphere packing density mentioned above, because the granule density and the granule packing are both below D_{RDP}.

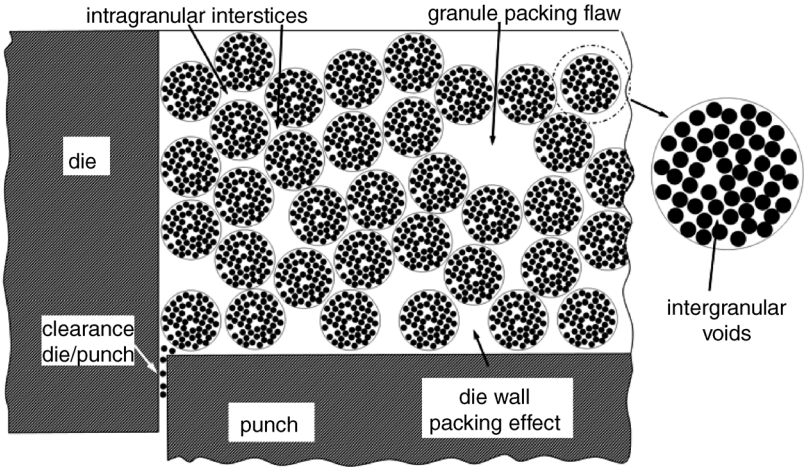

Figure 1.4 Hierarchic packing structure of a press granulate.

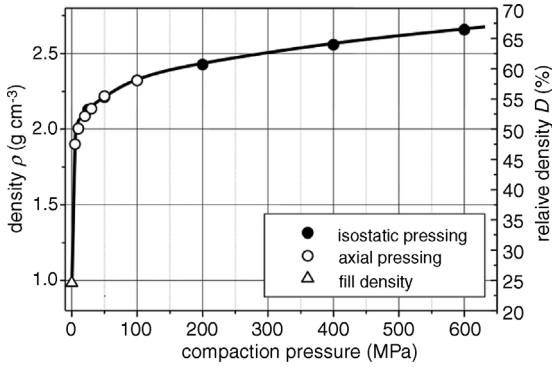

Figure 1.5 Pressure–density characteristics of granulated alumina powders.

1.2.2 Compaction Behavior

The primary characteristic of powder is the relative density achieved at a given compaction pressure, expressed in the form of a pressure–density plot, as illustrated in Figure 1.5. The mean density starting from the filling density initially increases rapidly, then saturates at high pressure. The compaction pressure p used in these plots is the macroscopic "technical" compaction pressure, usually derived from die-pressing experiments in which p is simply the load F acting on the punches, divided by the cross-sectional area A of the compact:

$$p = \frac{F}{A} \tag{2}$$

The state of stress and the stress distribution in the compact are not taken into consideration. The compaction behavior of monolithic (metallic) powders and ceramic granulates, both of which can plastically deform, are described in the following subsections, together with discussions of the state of stress, advanced modeling, and the practice of uniaxial compaction.

1.2.2.1 Compaction of Monolithic Powders

The compaction process can be roughly divided into three stages:

- In stage I, the density increases from the filling density to the RDP level of the powder.
- In stage II, where the particles stay surrounded by interconnected pores, the density increases by pore reduction to reach 80–90%.
- In stage III, the pores are sealed off and the material behaves like a solid with isolated pores.

The mechanisms that control densification include particle rearrangement, the plastic deformation of particle contacts, and fragmentation of the particles. In principle, rearrangement is the only mechanism until RDP is reached. Further

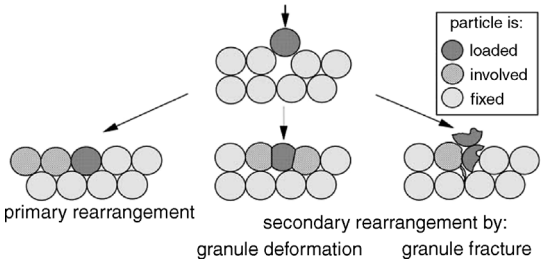

Figure 1.6 Primary versus secondary rearrangement.

densification definitely requires a shape accommodation of the particles by plastic deformation or fragmentation. In practice, these mechanisms overlap, with primary rearrangement occurring when the bridging stresses are low and when the void entrances can open (to accommodate new particle fill-in) by the displacement of neighboring particles. If the bridging stresses are beyond the yield or rupture strength, then a secondary rearrangement takes place (Figure 1.6). Consequently, rearrangement is also contributing at density levels above RDP, whereas plastic deformation and fragmentation may already be required at density levels below RDP.

The analytical micromechanical models for these mechanisms that were developed during the 1970s provide a good basis for understanding compaction behavior [22–24]. The stage II models assumed a RDP of monosized spheres under isostatic pressure, and analyzed representative particle contacts. As the contact stresses exceed the material's yield strength, the particle contacts are plastically deformed to reduce the center-to-center distance between particles, and hence the density increases. In the meantime, the contact area increases, which in turn decreases the contact stresses, until the contact stresses are balanced by the yield strength. This "geometrical hardening" factor explains the diminishing slope of the pressure–density relationship, even for perfectly plastic materials with a constant yield strength. For materials with work-hardening behavior (such as metals), the degression of the slope is even stronger. Instead of considering the deformation of particle contacts, the stage III models [beyond about 90% of theoretical density (TD)] focus on the more realistic picture of yielding a continuum with isolated pores, which shrink in size if the stress in the surrounding material shell exceeds the yield strength. This approach results in the theoretical master curve for compaction [Eqs (3) and (4)], which scales with the yield strength σ_y as plotted in Figure 1.7. As expected, a compaction pressure of $P \approx 3\sigma_y$ is sufficient to come close to theoretical density. It is interesting to note that, in semi-logarithmic coordinates, the shape of this curve is not far from that observed for ceramic granulates (see Figure 1.9).

$$p = 3 \cdot D^2 \left(\frac{D - D_0}{1 - D_0} \right) \cdot \sigma_y \quad D_0 \leq D \leq 0.9 \tag{3}$$

$$p = \frac{2}{3} \sigma_y \ln \left(\frac{1}{1 - D} \right) \qquad 0.9 < D \leq 1.0 \tag{4}$$

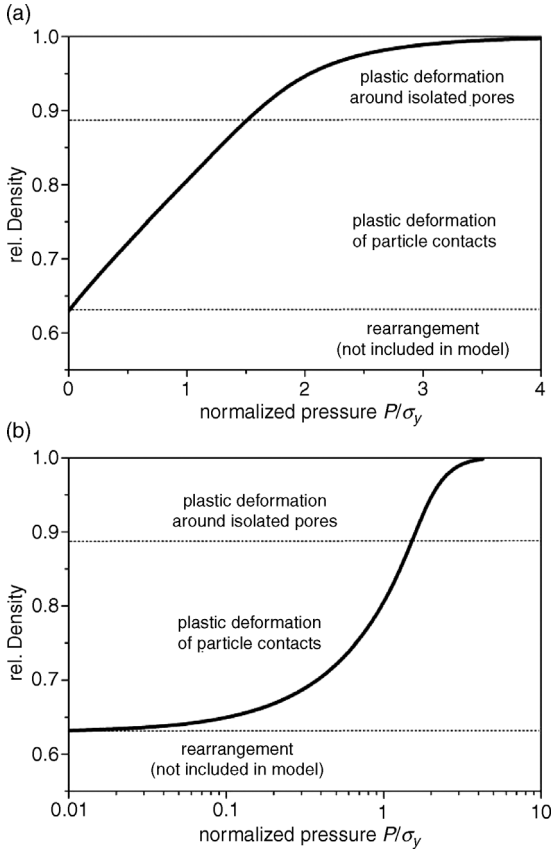

Figure 1.7 Pressure–density plots for monolithic monosize spheres, derived from analytical micromechanical models in (a) linear and (b) semi-logarithmic coordinates. σ_y is the material's yield strength; calculations made according to Ref. [24].

1.2.2.2 **Compaction of Granulated Powders**

Ceramic granulates consist of agglomerated primary particles, which are weakly bonded by organic pressing aids. Due to the viscous behavior of the pressing aids, ceramic granulates are sensitive to deformation rates, unlike monolithic metallic particles, and this limits the compaction rates for ceramics. In the case of poor powder processing – for example, with insufficient milling – the primary particles can also form aggregates, which are strongly bonded subunits of the granules. Ideally, the granules should be spheres with a desired size, and weakly bonded primary particles not far from RDP packing, which ensure a good deformability. This can be achieved more or less by applying common granulation methods.

The fill density of some technical powder granulates (data from Refs [25] and [26]) is illustrated graphically in Figure 1.8; typically, this will be in the range of about 20–35%, and the granules will have densities ranging from about 30% to 60%. According to Eq. (1), these data indicate granule packing densities between 50% and

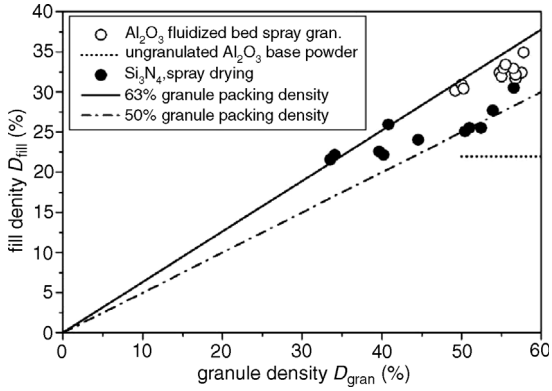

Figure 1.8 Fill density versus granule density of ceramic granulates (data from Refs [25, 26]).

63%, comparable to that of monolithic powders. Although the overall fill densities (20–25%) seem to be rather low, they still significantly exceed the fill density of the base powders, which have micron or submicron sizes.

In general, problems arise not from the low fill density of granulated powders, but rather from the hierarchical void structure of the particle packing. There are three classes of void: (i) the interparticle voids between the primary particles; (ii) the intragranular voids between the granules; and (iii) larger packing flaws (see Figure 1.4). If this compact is sintered directly, there would be densification and grain growth inside the granules, while the large intergranular voids and packing flaws would remain essentially unaffected. Therefore, compaction is essential in order to eliminate the packing flaws and to reduce the size of the intragranular voids to that of the intergranular voids.

Compaction involves the stress-induced rearrangement and deformation of the granules. Rearrangement depends on the initial granule packing structure, and the granule size distribution and hardness. Granulates with a high flowability and low intergranular friction have fewer packing flaws after rearrangement. In addition, the filling of packing flaws by rearrangement is favored by hard granules [27]. Granule deformation varies from being brittle to plastic, depending on the size distribution and shape of the primary particles, the amount, nature, and local distribution of the pressing aids, and the internal structure of the granules. Granule size, however, has little influence.

For a given compaction pressure, soft granules lead to higher compact densities than hard granules. In analogy to monolithic (metallic) powders, the yield strength of the granule is the controlling property for granule deformation, at least for non-brittle granules. Following Lukasiewicz [28], a "granule yield pressure" is often determined from semi-logarithmic pressure–density plots in which agglomerated powders show two or three linear regions separated by sharp breaks (compare Figure 1.9). Rearrangement is believed to control compaction in the low-pressure linear region, whereas deformation or fracture (in the case of brittle granules) dominates in the medium-pressure region. The lower break point pressure (1. BPP) is identified as the yield or fracture strength of the granules, and this correlates with the hardness of

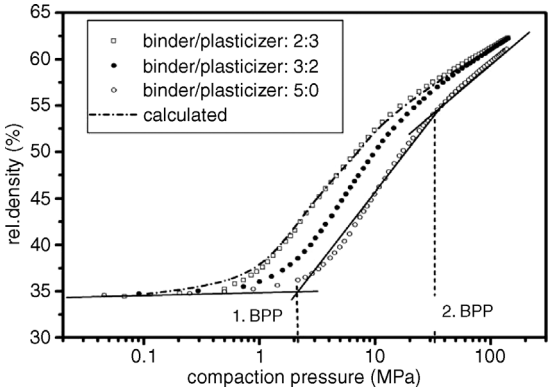

Figure 1.9 Pressure–density plots of monosize alumina granulates. Granule yield strength is varied by the binder : plasticizer ratio (data from Ref. [26]).

the granules. A direct examination of the compacted and fractured compacts showed that the granules were not destroyed before the first break point, but extensive plastic deformation had occurred at pressures higher than this break point [7]. After the second break point pressure (2. BPP), transition into the high-pressure linear region with a lower slope proceeds by the intragranular compaction of granules. Ideally, all intergranular voids are eliminated and the compact density reaches the initial granule density at this 2. BPP.

Experimental semi-logarithmic pressure–density plots for monosized alumina model granules are shown in Figure 1.9 [26]. Here, the granule hardness was systematically varied by the binder : plasticizer ratio of the pressing aids; three linear sections can clearly be identified, with lower break point pressures between 0.8 and 3 MPa. Parameters derived from single granule compression tests, such as the single granule fracture strength $\sigma_{c,\mathrm{sg}}$ or the single granule yield strength $\sigma_{y,\mathrm{sg}}$, exceeded these values by a factor of between 2 and 10. The second break point occurs at density levels somewhat below the initial granule density, which ranged from 55 to 57%. Therefore, the explanation of the mechanisms associated with the break point pressures seems to be questionable.

Pressure–density curves were calculated using Eqs (3) and (4), and employing the measured single granule yield strength values. The computed curves match the experimental values from Figure 1.9 in stages I and III, but deviate strongly in the middle linear region of stage II (not shown in Figure 1.9). A good agreement (see the curve "calculated" in Figure 1.9) was achieved with an empirical fit, which uses a density-dependent apparent yield strength $\sigma_{y,\mathrm{app}}$ according to Eq. (5). The so-derived apparent granule yield strength is shown in Figure 1.10 as a function of normalized density (compact density divided by initial granule density).

$$\sigma_y = \sigma_{y,\mathrm{sg}} \cdot \left(0.36 + 14.5\left(\frac{D - D_{\mathrm{fill}}}{D_{\mathrm{gran}}} D\right)^2\right) \tag{5}$$

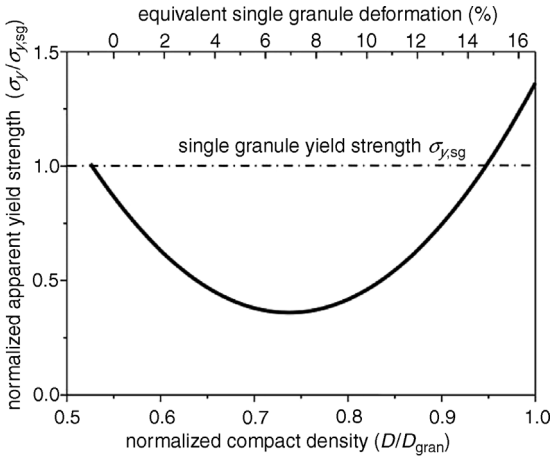

Figure 1.10 Normalized apparent yield strength derived from fitting experimental pressure–density curves to the Fischmeister model [22] ($\sigma_{y,app}$ is normalized by the measured single granule yield strength $\sigma_{y,sg}$).

This indicates that the single granule yield strength $\sigma_{y,sg}$ is a suitable parameter at the onset of stage II. It is derived from the single granule load–deformation curve by an often-used analytical solution for the center-to-center approach of two perfectly plastic spheres [22, 26]. With increasing granule contact deformation, the resistance against deformation is decreased as cracks develop in and below the contact planes caused by tensile stresses generated by a partial intrusion of the deformed material into the granules. The minimum deformation resistance is observed when the compact reaches about 75% of the initial granule density, beyond which the deformation resistance recovers. At a normalized compact density of 100%, the deformation resistance well exceeds $\sigma_{y,sg}$ indicating an apparent "compact hardening." The latter is due to a suppression of crack formation when the granule is surrounded by other granules; this causes a hydrostatic stress to develop, especially at higher density with an increasing number of granule–granule contacts. According to this model, the individual granules are deformed by less than 20% when the compact density reaches the initial granule density (normalized density = 100%). Therefore, despite the simplicity of the model and the idealization of monosized spherical granules, the findings allow a qualitative understanding of the compaction behavior of ceramic granulates.

If the granules are incompressible, then the maximum density is the initial granule density, which is reached when the intergranular pores are completely eliminated. Further densification is possible if the primary particle packing structure in the granules allows for rearrangement by particle sliding, and this is the case for lower granule densities. Densely packed primary particle arrangements can be further densified only by plastic deformation or cracking of the primary particle contacts, which is difficult for ceramic materials. Indeed, although aggregate/granule fracture is common, the fracture of primary particles is rarely seen [7].

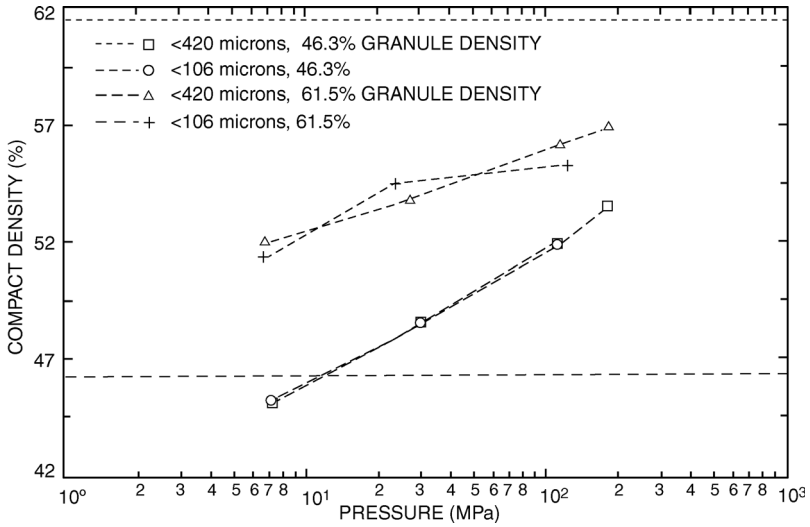

Figure 1.11 Density–pressure plots for alumina powder prepared at two levels of granule density [29]. Reprinted by permission from American Ceramic Society; © 1988.

As a rule of thumb, granulates should be compacted at least to the level of initial granule density. To obtain a homogeneous compact structure, granules with densities somewhat below the theoretical packing density of the underlying particle system can be more suitable than dense primary particle structures, because the intergranular voids can be eliminated at lower compaction pressures, as shown in Figure 1.11 for alumina granulates [29].

This is counterbalanced by negative effects, such as a reduced filling density. As the compact density remains below the level achieved with the denser granules over the range of practical compaction pressures (Figure 1.11), the granule density should have an optimum value. This applies also to the granule yield strength or hardness. Hard granules are difficult to deform, and this results in lower densities at a given compaction pressure, as shown above. However, if the granules are too soft they will deform readily under pressure, but will not rearrange sufficiently at low pressure. Some packing flaws, which are not completely filled during the deformation stage, will remain and large density gradients will be formed in uniaxial pressing [27]. Ideally, the granules undergo rearrangement as well as deformation during compaction [9].

If the granules are not sufficiently deformed during compaction, then intergranular pores and surviving granule interfaces will cause granulate-related defects in the sintered parts. Typically, such granule relicts are especially pronounced at flat or convex surfaces, where the granules are not surrounded on all sides by neighboring granules; an example is shown in Figure 1.12.

1.2.2.3 **Understanding Powder Compaction by Advanced Modeling**

Progress in numerical modeling during the past two decades has contributed significantly to a much more detailed understanding of compaction behavior, beyond

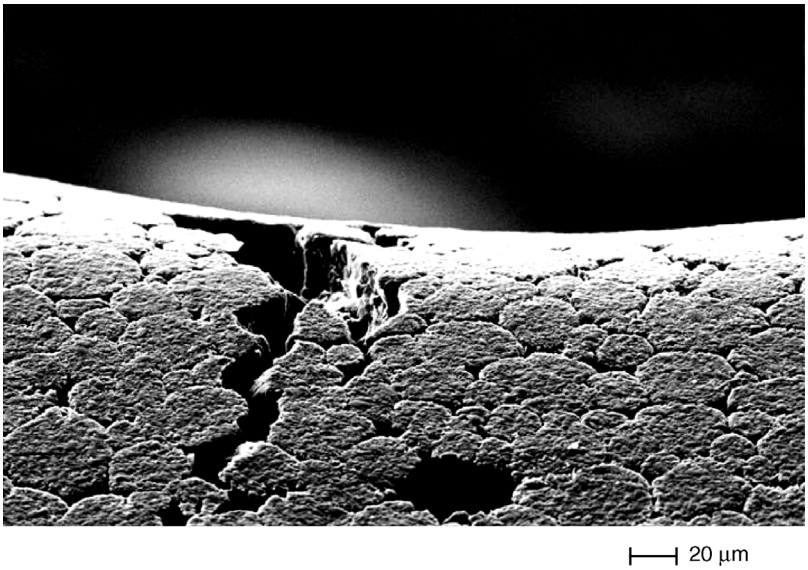

Figure 1.12 Granule-related defects at the surface of a ceramic part. The insufficiently deformed granule interfaces caused a crack in the green compact, which opened during sintering.

the earlier analytical micromechanical models (for reviews, see Refs [30, 31]). The models are classified as either:

- *phenomenological models*, which are based on continuum soil mechanics, and are adopted to simulate the pressing of real parts by finite element methods (FEM); or
- *micromechanical models*, which derive the bulk powder properties by modeling the interactions between powder particles.

The micromechanical models can be further subdivided into two methods [32]:

- The discrete element method (DEM) is based on a local model of the contact behavior between two particles, where the relationship between the normal contact force and the displacement is of major importance. Tangential forces are included, and contact friction mechanisms are taken into consideration. The DEM models are able to reproduce particle rearrangement. However, as such models assume that the individual contact zones do not interact, their application is limited to stage I and stage II compaction in the density level of $D < 0.8$.
- The meshed DEM (MDEM) is based on FEM simulations of meshed discrete particles, which are arranged as periodic structure, or two-dimensional (2-D) or even 3-D random packings. Although MDEM methods produce accurate results up to high densities, the simulation is limited to assemblies of approximately 100 particles.

Effective modeling requires a combination of the different methods. On a first level, MDEM can be used to derive force–displacement laws for DEM [32], whereas on a second level DEM simulations can be used to derive suitable constitutive

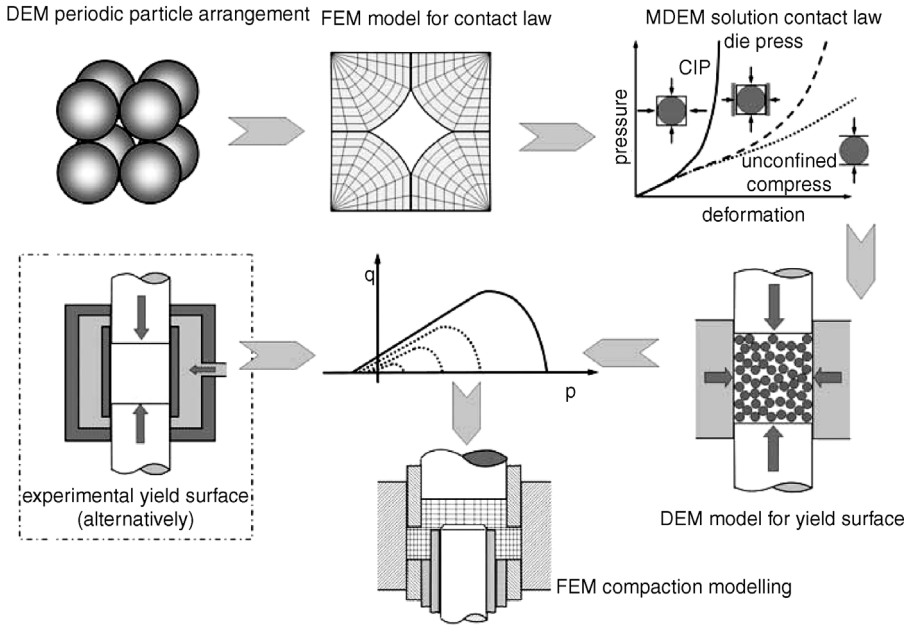

Figure 1.13 Modeling methods for powder compaction.

equations. On a third level, the compaction of a real compact can be simulated by employing FEM calculations using these constitutive equations (Figure 1.13).

Numerical DEM simulations of stage I compaction can model loose packing configurations, particle size distributions [33] and composite powders with different material strengths and sizes [34]. An important finding here is that the force transmission during the packing is inhomogeneous, and at any given moment only a fraction of the particles carries the load to support external pressure. Due to computing time restrictions, the simulation of a whole part is not feasible with DEM models; rather, their relevance derives from their ability to identify (in small volume elements) the microstructure development as a function of fundamental materials parameter and boundary conditions. As the stress state can be easily varied, DEM can be used to derive constitutive equations (yield surfaces), to be used as the input for phenomenological models, which simulate the compaction of complex parts [35].

DEM simulations of agglomerated powders with weakly bonded primary particles, and aggregated powders where the primary particles were bonded by solid bridges [36, 37], support the concept of cracking as part of the contact deformation mechanism mentioned above. The strength of agglomerates was found to be approximately inversely proportional to the primary particle size, thereby confirming Rumpf's equation [38] that was derived during the 1970s. The agglomerate strength is increased from about 1 MPa for 1-μm primary particles to 200 MPa for 10 nm particles (Figure 1.14). For strongly bonded aggregates, the primary particle size becomes relevant only if it is well below 100 nm. With an assumed fracture stress of

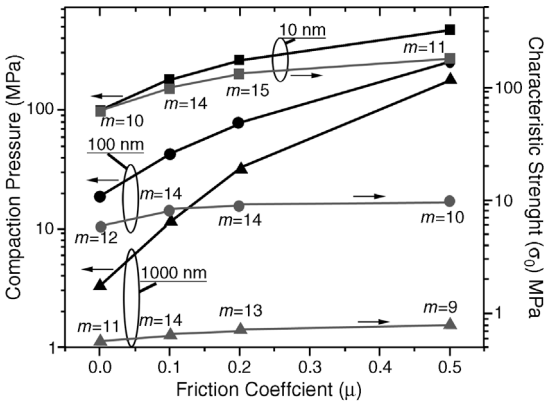

Figure 1.14 Left-hand scale: Compaction pressure at 0.60 relative density under uniaxial compaction conditions as a function of the interparticle friction coefficient; μ. Right-hand scale: Characteristic strength for individual agglomerates made of 500 primary particles [37]. Reprinted with permission from Elsevier; © 2010.

the solid bridges of 2 GPa, the aggregate strength is calculated to be ~80 MPa (which is less than the corresponding agglomerate strength) for 10-nm primary particles, and ~30 MPa for 100-nm to 1-μm primary particles. The simulated pressure–density relationships, showing similar shapes to the curves in Figure 1.9, are all in fair quantitative agreement with experimental results. Besides the primary particle size, the friction between the primary particles is an important parameter. For 1-μm primary particles, the compaction pressure required to densify the compact to 60% of theoretical density is reduced by a factor of 50 when the interparticle friction coefficient is reduced from 0.5 to 0. In the case of 10-nm particles, however, the reduction is only a factor of 5 (Figure 1.14). The primary particle size and interparticle friction are, therefore, the most important parameters for ceramic granulates.

Besides powder compaction, DEM models are used to provide an understanding of, or predictions for, die filling. A recent 3-D-DEM modeling of the filling of a ring-shaped die cavity was shown to agree fairly well with experimental results [39]. Although such calculations require very high computational power, they have great application potential, an example being the optimization of design for the powder filling cycle [40]. DEM has also been combined with computational fluid dynamics (CFD) to include air flow in filling simulations [41]. The influence of particle size, particle density, polydispersity and attractive interparticle forces on die filling has also been investigated.

The phenomenological compaction methods [42, 43] were originally developed for soil mechanics in continuum plasticity. The material response is expressed in terms of stress and strain invariants, for example, the hydrostatic pressure, p, and the von Mieses equivalent stress, q. The hydrostatic stress p is the mean of the principal stresses σ_{ii}:

$$p = \frac{\sigma_1 + \sigma_2 + \sigma_3}{3} \tag{6}$$

The equivalent stress is given by:

$$q = \frac{1}{3}\left[(\sigma_1 - \sigma_2)^2 + (\sigma_2 - \sigma_3)^2 + (\sigma_3 - \sigma_1)^2\right]^{\frac{1}{2}} \tag{7}$$

For a cylindrical compact subjected to an axial stress σ_a and a radial stress σ_r (Figure 1.15) this reduces to:

$$p = (\sigma_a + 2\sigma_r); \quad q = (\sigma_a - \sigma_r) \tag{8}$$

The elastic deformation ε_i is given by:

$$\varepsilon_v = \varepsilon_a + 2\varepsilon_r = \frac{p}{K} \quad \varepsilon_e = \frac{2}{3}(\varepsilon_a - \varepsilon_r) = \frac{q}{3G} \tag{9}$$

where K is the bulk modulus, and G the shear modulus. The hydrostatic stress (pressure) densifies the volume, while the equivalent stress distorts the volume.

Plastic deformation occurs when the stress reaches the yield surface, which is a convex in the stress space. This surface depends on the stress invariants p, q, and the current state of the material (mainly the density of the compact). The most often-used model in FE simulations is the Drucker–Prager Cap (DPC) model, as included in Figure 1.15. Compact density has a major influence on this yield surface, which expands with densification. At stress levels within the yield surface, the compact deforms elastically; subsequently, when the stress level reaches the boundary, yielding takes place and the result is plastic deformation. Incremental deformation – that is, the strain vector – is in the direction normal to the surface. A positive component of the strain vector in the p-direction results in densification, while a negative component will result in (dilatant) shear failure.

With a corresponding flow rule, deformation – and thus compaction – can be calculated incrementally for large and complex parts by using FE methods. The main applications of this are in the tool design for complicated multilevel parts. The required constitutive laws can be derived from triaxial compaction experiments [44, 45], the model fitting of special axial compaction experiments [46], or via DEM models.

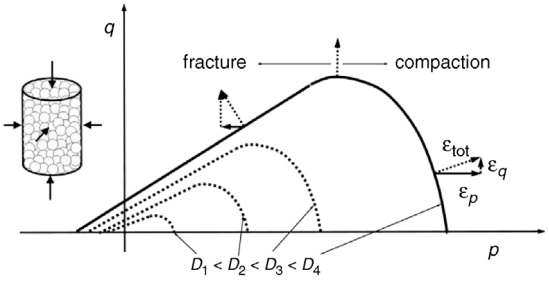

Figure 1.15 Yield surfaces for different density levels on the p–q-plane.

1.3
Practice of Uniaxial Compaction

Axial pressing [4] is the most important forming method used for ceramic parts. In this process, the powder is compacted between rigid punch faces and die walls, which in turn allows the compacts to be fabricated to very close geometric tolerances. The compaction sequence – which consists of die filling, compaction, and ejection of the compact – is carried out on mechanical or hydraulic compaction presses, which enables high production rates. Consequently, axial powder pressing is a very economic method that can be used for the mass production of precision parts such as cutting tool inserts and sealing disks.

1.3.1
Die Filling

Two general systems are used for die filling:

- A *mass-controlled pre-dosing system*: nowadays, such systems are very rarely applied to ceramic materials.
- A *volume-controlled feed shoe system*: this consists of a bottomless box feed shoe that is pressed onto the die platen and slit over the open die, and a hopper from which the powder is fed under gravity into the feed shoe. When the die is filled, the feeder is pulled back into a resting position. For complex or thin-walled parts, the fill shoe and tool movements are controlled to realize overfilling, suction filling, or contour filling, so as to improve the density distribution of the compacts (Figure 1.16) [10].

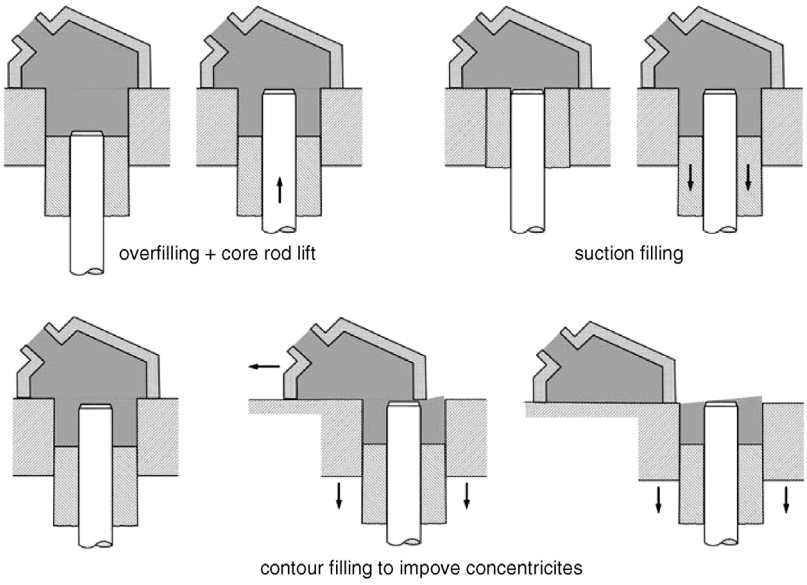

Figure 1.16 Die filling methods used in axial powder pressing.

An incorrect die filling can lead to inhomogeneities which, depending on the die geometry, may not be smoothed out during compaction. The uniformity of die filling has been reviewed [47]. In addition to the powder and the cavity dimensions, filling depends on the feed shoe velocity, with a critical fill shoe velocity v_{crit} being observed experimentally for each distinct type of powder, including ceramic and hardmetal granulates [48, 49]. Whilst the die is completely filled by a single pass of the shoe below v_{crit}, filling will be incomplete at higher velocities (Figure 1.17). At $v > v_{crit}$, the fill ratio δ is decreased, according to the empirically derived Eq. (10):

$$\delta = \left(\frac{v_{crit}}{v}\right)^n \tag{10}$$

The critical velocity can be approximated from the so-called Beverloo equation, which originally was derived to determine hopper flow. If the granule size is much lower than the die opening, then this equation can be rewritten as:

$$\dot{m} = C \cdot \varrho_b \sqrt{g \cdot D_H} \cdot A \tag{11}$$

where C is a constant, g is gravity, D_H is the hydraulic diameter of the die cavity, and A is the cross-sectional area. v_{crit} is given by:

$$v_{crit} = C \cdot \sqrt{g \cdot D_H} \cdot \frac{l}{h} \tag{12}$$

where h is the height and l is the length of the filling shoe. For lower shoe speeds, a value of C of about 0.14 was determined for several powders [48]. At low speeds, the so-called "nose flow" (Figure 1.17) is dominant and the cavity will be filled mainly with powder from the top of the shoe. The critical velocities in air are nearly the same as under vacuum. At high speeds or with small die openings, however, the powder is detached from the bottom free surface by bulk flow. The critical velocities are significantly higher in air than in vacuum, as air flow effects caused by entrapped air will influence the filling. Modifications to the Beverloo equation made in Refs [49] and [39] provide more sophisticated analytical expressions for v_{crit}.

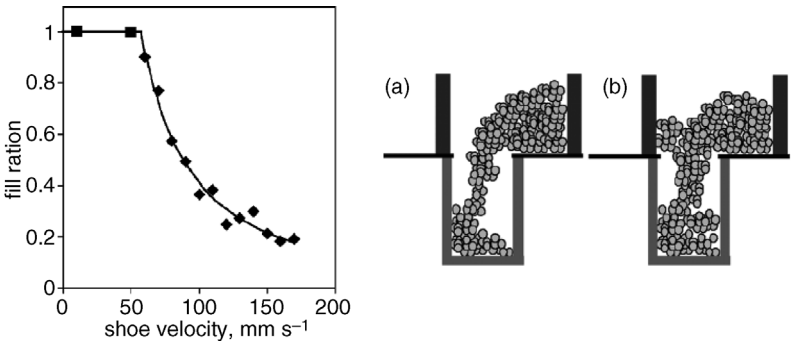

Figure 1.17 Die filling behavior of powders. Left: Critical fill shoe velocity (iron powder). Right: Schematic representation of (a) nose flow, (b) bulk flow [49]. Reprinted with permission from Maney Publishing; www.maney.co.uk/journals/pom, www.ingentaconnect.com/content/maney/pm.

The influence of particle size, particle density, polydispersity and attractive interparticle forces on die filling, with entrapped air, has been studied by employing a combined DEM and CFD simulation [41]. For this, a stationary filling shoe with a shutter was considered in the simulations, and two distinct regimes have been identified: (1) an air-sensitive regime for smaller particles and lower material densities; and (2) an air-inert regime for larger particles and higher material densities. Due to air flow, the powder volume flow rate increases with particle size and density within the air-sensitive regime, but it is identical with the flow rate in vacuum within the air-inert regime. In the latter case, the flow rates are in fair agreement with the Beverloo equation, whereas in the air-sensitive regime they are strongly reduced. Polydispersity and adhesion appear to have only a minor influence within the investigated parameter range.

1.3.2
Tooling Principles and Pressing Tools

For simple parts, the pressing tools consist of a die and an upper and a lower punch, whereas more complicated parts require the use of mandrels and splitting of the punches. In special cases, split dies may also be applied. The parameters which determine the required tooling include the compact geometry, the filling and compaction factor, and the acceptable density gradients in the compacts. Density gradients result from differences in the compaction pressure inside the compact, due mainly to wall friction effects. The problem of die wall friction is demonstrated in Figure 1.18 for a compact under single-action compaction. Assuming the same axial pressure p_{ax} over the cylindrical cross-section of a diameter d, p_{ax} can be calculated as a function of the distance z from the upper punch, according to Eq. (13):

$$p_{ax}(z) = p_{ax,0} \cdot \exp\left(-4 \cdot \mu \cdot k \cdot \frac{z}{d}\right) \tag{13}$$

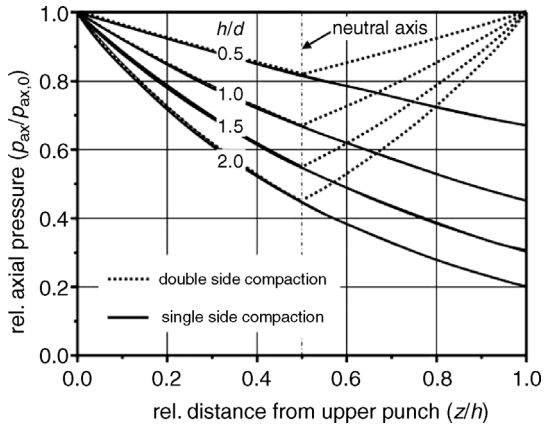

Figure 1.18 Normalized axial compaction pressure as function of the normalized distance from the upper punch surface.

where $p_{ax,0}$ is the pressure at the upper punch surface, μ is the friction coefficient which depends on the wall roughness and lubrication, and k is the radial pressure coefficient (ratio of axial to radial pressure), which depends on the internal friction of the particles and is lower for irregular or unlubricated powders. For typical ceramic press granulates, k is in the range of 0.4–0.5 [7].

Figure 1.18 indicates the pressure drop for values of $\mu = 0.5$ and $k = 0.4$ and different height (h) to diameter (d) ratios for the compact. Even for equiaxed compacts with (h/d)=1 the pressure at the lower punch is less than half of the upper punch compaction pressure. For more complex tools with core rods, (h/d) is replaced by ($A_{\text{punch}}/A_{\text{mantle}}$), where A_{punch} represents the pressure-transmitting end face of the punch, and A_{mantle} is the mantle surface of the compact.

One major drawback of single-action compaction is the unsymmetrical density gradient, which leads to warping of the compacts during sintering. This problem can be significantly reduced, however, if the compaction pressure is allowed to act on both punches. This so-called "double-action pressing" is schematically compared to single-action pressing in Figure 1.19. In single-action pressing, the density decreases from the top to the bottom of the compact according to Eq. (13), whereas in double-action pressing the axial pressure is symmetrical to the central cross-section of the compact, the so-called "neutral axis" or plane. The minimum pressure and density are found in this plane. The height/diameter ratio in Eq. (13) is formally reduced by a factor of 2 for double-action pressing, which in turn significantly reduces the pressure gradients, as shown in Figure 1.18.

The tooling principles used in uniaxial pressing are described schematically in Figure 1.20. Double-action pressing is applied for the majority of parts, even those with a low height/diameter ratio. With a stationary die (Figure 1.20a and b), the compaction force is applied simultaneously to the upper and lower punch. The same double-action effect can also be achieved with a floating die (Figure 1.20c) that is mounted on springs which balance the weight. In this case, as the wall friction forces cause the die to move down, the force on the lower stationary punch increases until the frictional forces from both punches come into equilibrium. This principle is often used with laboratory presses. The withdrawal tooling system (Figure 1.20d) utilizes a moving die that is actively controlled, the aim being to keep the neutral axis in the

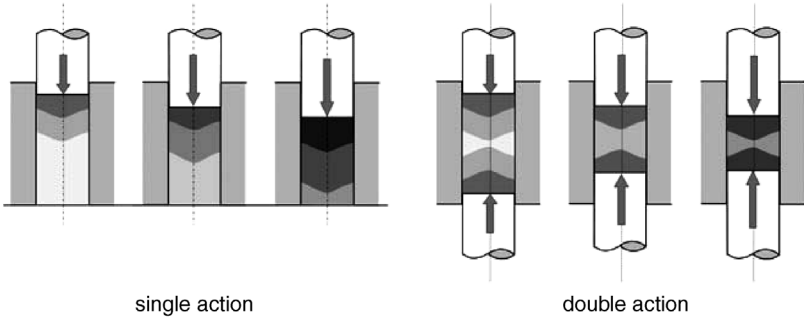

Figure 1.19 Uniaxial compaction: single-action versus double-action pressing.

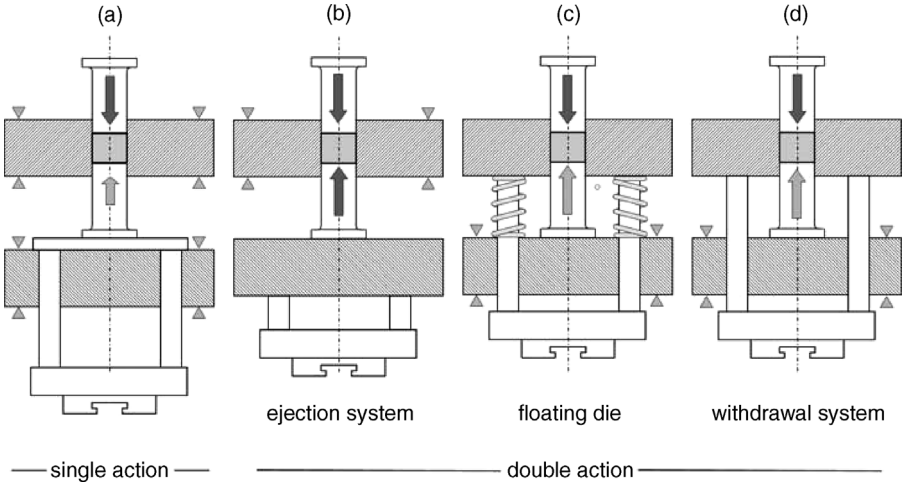

Figure 1.20 Tooling principles for uniaxial pressing. (a) Single-action pressing; (b) Ejection tooling system; (c) Floating die tooling system; (d) withdrawal tooling system.

center of the compact. Ejection of the pressed compacts is carried out by an upwards movement of the lower punch in the double-action and floating die systems, and by withdrawing the die in the withdrawal system. Although the withdrawal system requires a lower load capacity for the lower ram, both rams must provide the full compaction force with the ejection tooling system.

As material transfer perpendicular to the pressing direction is very limited, sectioning of the punches becomes necessary when producing compacts with more than one thickness level. This is shown in Figure 1.21 for a three-level part where, in the filling step, each section is filled with the required amount of powder. In the powder transfer step, the powder columns are transferred into their final relative position. Compaction during this step would lead to pressing defects, and is therefore avoided. In the compaction step, the individual punch sections ideally should move in such a way that the neutral axis remains in the center of each section.

A complete pressing tool can consist of a variety of upper and lower punches, core rods for forming through holes, the die, and a die set (adapter) on which the components are mounted. The use of such die sets increases production flexibility, as the time required to change a complete tooling system is relatively short. The limitations of the system are that parts with features perpendicular to the pressing direction cannot be compacted and stripped (e.g., parts with cross holes and threads). However, sophisticated tooling and advanced control technology can help to overcome these problems [10].

1.3.3
Powder Compaction Presses

Specialized mechanical, hydraulic, hydraulic–mechanical or direct electrically driven powder presses are generally used in dry pressing [50]. A recent review of

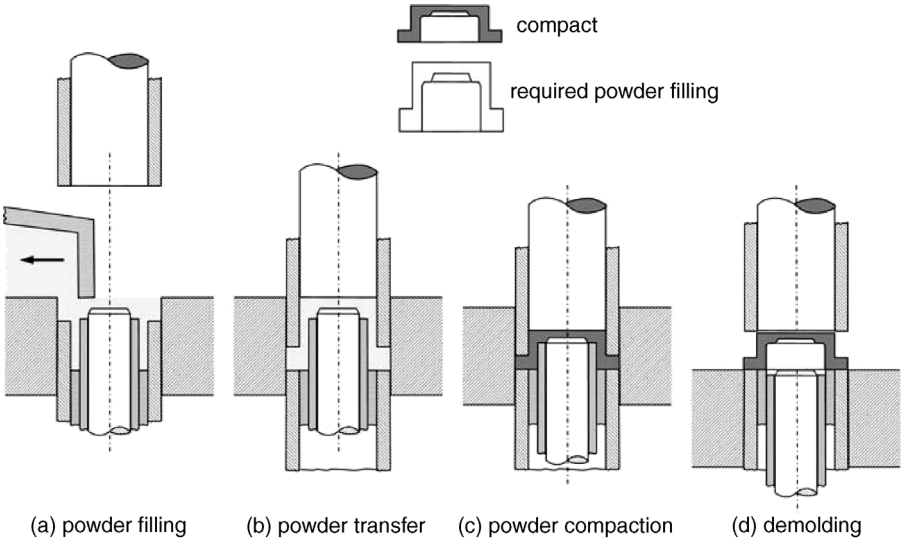

Figure 1.21 Tooling and compaction sequence for a three-level part. (a) Powder filling; (b) Powder transfer; (c) Powder compaction; (d) Ejection of the part by withdrawal of the die (demolding).

hardmetal and iron powder pressing technology [10] is also mostly applicable to ceramic powders. In general, cam-driven mechanical presses have pressing capacities of about 1 MN, while the typical capacity of eccentric mechanical presses ranges from about 7 kN to 7.5 MN; by comparison, standard hydraulic press capacities range between 120 kN and 20 MN. A more recent development has been the direct electrically driven press, which may have a capacity of up to 160 kN pressure. The production rate of mechanical presses is generally greater than that of hydraulic presses (by a factor of between 1.5 and 5), while their maximum stroke rates are about $6000\,h^{-1}$ and $650\,h^{-1}$, respectively. Hydraulic systems are generally best suited to producing high compacts. Their maximum depth of powder fill is about 400 mm, compared to 200 mm in a standard mechanical press. Modern hydraulic presses employ computer-controlled servo hydraulics that provide not only very precise punch movements but also an ability to control the pressing sequence of multiple punch tooling systems in very effective fashion. Typically, up to 15 closed-loop controlled axes are provided to actuate the rams, core rods, auxiliary platens, the powder filling system and side compaction units. This permits parts with cross holes and undercuts to be produced, that cannot be prepared with conventional die pressing.

In axial pressing, failure occurs if the ejection shear stresses in the compacts exceed the green strength. Ejection shear stresses are caused when a compact expands as it leaves the die, and they increase in line with increasing compaction pressures. In the die pressing of ceramics, this places a limit on the maximum safe compaction pressure, typically to a level of 100–200 MPa.

1.4
Practice of Isostatic Compaction

Cold isostatic pressing is a powder-forming process [51, 52] where compaction takes place under isostatic or near-isostatic pressure conditions. Two main process variants exist, namely wet-bag and dry-bag isostatic pressing. In both techniques, the powder is first sealed in an elastomeric mold, which is then pressurized by a liquid, such that the powders become set under (hydrostatic) pressure. Typically, pressures up to 400 MPa are used on an industrial scale, although some laboratory equipment is designed to operate at pressures up to 1 GPa. The pressure medium must be compatible with the tool, the vessel, and the pumping system. In practice, special oils, glycerin or water with anticorrosive and lubricating additives are used. As these fluids are not incompressible at high pressures, they can store considerable elastic energy and, consequently, safety aspects must be considered when designing and operating the pressing equipment.

Wet-bag isostatic pressing requires extensive handling, and is used mainly for the production of prototypes or the low-volume production of parts. In contrast, dry-bag isostatic pressing is a mass production process; an example is the production of spark plug insulators, for which several million must be produced worldwide on a daily basis. The main advantages of isostatic pressing are that it produces a much more uniform density distribution than does uniaxial pressing, and the ejection stage – which often causes pressing defects – is avoided. One disadvantage, however, is the lower geometric precision of the compacts.

1.4.1
Wet-Bag Isostatic Pressing

In wet-bag pressing, the tool (bag/elastomer mold) is filled with the powder and sealed, after which the bags are placed into the pressure medium inside a pressure vessel that is then closed and pressurized. A controlled depressurization is carried out to avoid defects caused by the expansion of the elastomeric mold. The tooling used differs considerably from axial pressing tools (Figure 1.22). In the simplest case, a tool or mold consists of an elastomer mold while, for the fabrication of hollow parts such as tubes, the tooling includes rigid internal mandrels or other forms of support. Depending on the tool design, local deviations from isotropic densification may occur. Typically, the compact surfaces formed against the rigid parts of the tooling will have surface qualities and geometric tolerances comparable to those achieved in axial die pressing, whereas the surfaces formed against the flexible mold tend to exhibit greater tolerances and poorer surface qualities.

The molds will have the shape of the desired compacts. In the ideal case of isotropic shrinkage, the mold dimensions or the bag dimensions $d_{o,fill}$ (outer diameter of powder filling) are calculated from the compact diameter d_{comp} and the compaction ratio (the compact density D_{comp} to the fill density D_{fill} of the powder) by Eq. (14):

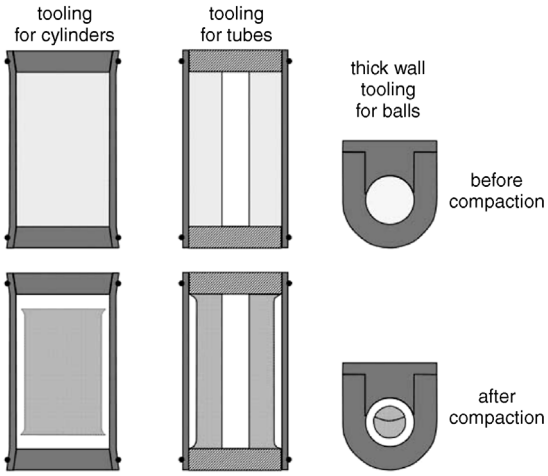

Figure 1.22 Examples of tooling and resulting compact shapes in wet-bag isostatic pressing.

$$d_{o,\mathrm{fill}} = d_{\mathrm{comp}} \cdot \sqrt[3]{\frac{D_{\mathrm{comp}}}{D_{\mathrm{fill}}}} \tag{14}$$

Another common case is a tool with a suppressed axial compaction, where densification takes place only in the radial direction and, as a consequence, Equation (14) changes to a square root. If such a tool contains stiff core rods, then the bag diameter will be larger for smaller inner diameters, and smaller for larger inner diameter. When the inner diameter exceeds about 70% of the outer compact diameter, the bag diameter will be smaller than that calculated from Eq. (14) (Figure 1.23).

Elastomers such as natural and synthetic rubber, silicone rubber, poly vinylchloride (PVC) and polyurethane are suitable bag materials. The criteria for material selection are compatibility with the pressure fluid, the stability of the mold, and the quantity of parts to be produced within the mold's lifetime. PVC and rubber molds, which can be produced by using simple dipping methods, are often preferred for single-use tooling, whereas polyurethane is the most common bag material for multi-use toolings. Unfortunately, polyurethane molds are relatively expensive due to the complicated casting method required for their production.

Wet-bag isostatic pressing offers several advantages compared to axial die pressing. Primarily, the shape capability is much less restricted so that parts with undercuts, through-holes and even internal threads can be manufactured. Due to an absence of die wall friction, thin-walled compacts with large height/diameter ratios can be produced. This differs from axial pressing, where the press capacity limits the maximum cross-section of the compacts to some hundreds of square centimeters; instead, the size limitations of wet-bag isostatic pressing derive from the dimensions of the pressure vessel. Currently, the largest systems in operation have dimensions of 2 m diameter and 3–4 m height, with a pressure capacity of 250 MPa.

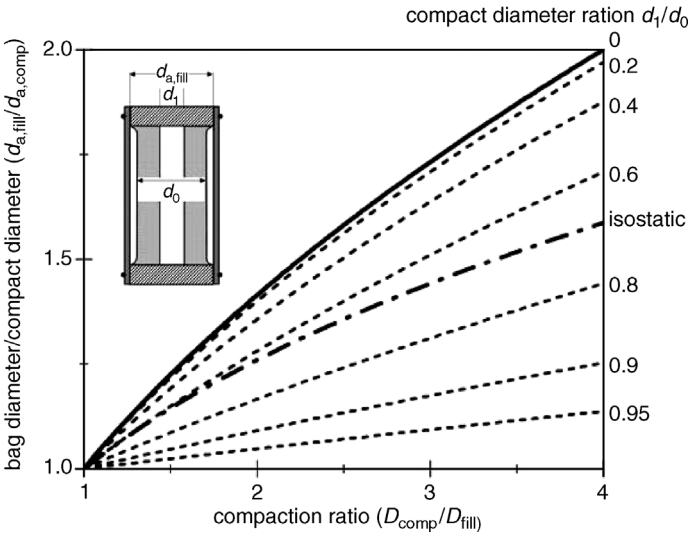

Figure 1.23 Ratio of bag diameter to compact diameter in dependence of the compaction ratio for toolings with stiff core rod in comparison to the case of isotropic shrinkage.

The homogeneous density distribution is responsible for a greater green strength and a more reproducible sintering shrinkage of the isostatically compacted parts. Although the absence of an ejection step is advantageous, the pressure must be released at a sufficiently low rate, as either the pore pressure caused by entrapped air or a relaxation of any sticking elastomeric mold can cause damage to the compacts. Other advantages include the relatively low tooling costs and the possibility to avoid die wall lubricants. The main disadvantages of wet-bag isostatic pressing are the higher dimensional tolerances (at least of the part sections formed by the flexible mold) and the long cycle times required (from 1 min to 1 h).

Today, wet-bag isostatic pressing is used in the commercial production of a variety of components such as filter elements, tubes, crucibles, milling or bearing balls, and of special structural parts with threads or undercuts that cannot be produced by die compaction. The process is also used widely in the production of blanks, which are shaped by machining them in their green or partially sintered state. Emerging applications are dental zirconia milling blocks, from which dental crowns and bridges are formed in the dental laboratory by using numerically controlled milling [53]. The need for a 20% shrinkage in the subsequent sintering step, and to preserve the required geometric dimensions, mean that wet-bag isostatic pressing must be used to maintain the density within a very narrow range, without any local variation.

Wet-bag isostatic pressing is a popular laboratory method for compacting ceramic powders, without granulation or the use of pressing aids. The technique is also applied for the re-pressing of green parts. Compacts, shaped either by axial pressing or by other forming methods, are first sealed using thin-walled elastomeric foils; re-pressing at an enhanced isostatic pressure will then increase the density and the homogeneity of the density distribution.

1.4.2
Dry-Bag Isostatic Pressing

In dry-bag pressing, a flexible membrane is built into the pressure vessel and used during all pressing cycles; the membrane separates the pressure fluid from the mold, which then becomes a "dry bag." This process, which permits rapid cycles, is very well suited to the automated mass production of powder products, the most prominent example being spark plug insulators. A typical dry-bag tool and the processing steps during the production of a spark plug insulator is shown in Figure 1.24. In step 1, the elastomeric mold is filled with the powder. The core rod, which forms the electrode channel of the insulator, is either already positioned in the mold or is inserted into the powder filling when the mold is closed. Pressurization of the pressing fluid in the compaction (step 2) generates a hydrostatic pressure inside the thick-walled elastomeric mold. When the pressure is released (step 3), the mold deforms back to its initial shape. Due to radial shrinkage, the compacted insulator blank can be withdrawn by lifting of the core rod (step 4). Other tooling systems use a reversed arrangement with the core rod at the bottom of the mold. In this case, the compacted part is ejected by an upward movement of the core rod.

Dry-bag isostatic pressing places high demands on the powder properties, with high flowability, high and reproducible filling densities, high compact green strength and an easy release of the compact surface from the mold and core rod being required. Therefore, granulation and well-designed additive systems are required for the dry-bag processing of micrometer or submicrometer ceramic raw powders.

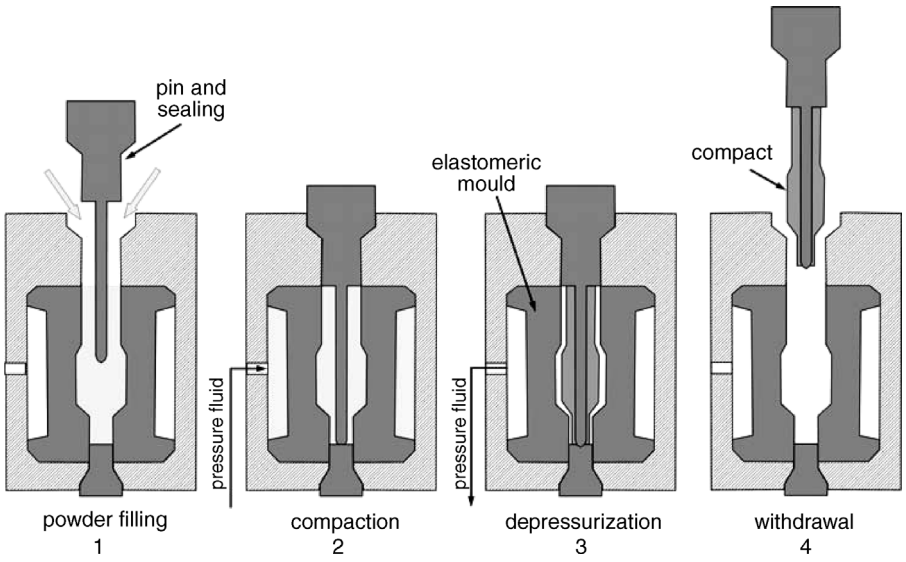

Figure 1.24 Production of spark plug insulators: dry-bag tooling and steps of the production process (see text for details).

Components such as spark plug insulators, milling and bearing balls, small ferrite parts, crucibles, wear parts, and thermocouple protection tubes are typical products of the dry-bag process. As the minimum cycle times are on the order of 1 s, very high production rates can be achieved with battery units that consist of several press cavities and a common control unit and pressure generator. Typically, 2800 pieces can be produced in 1 h using an eight-cavity unit at compaction pressures between 30 and 150 MPa [54]. Likewise, in a similar set-up the hourly production rate of ceramic grinding balls of 40 mm diameter may reach 10 000 units.

1.5
Granulation of Ceramic Powders

For the production of technical ceramics, the poor flowability of the micron or submicron powders makes it necessary to form press granulates by the controlled agglomeration of the primary particles. Granulation methods can be divided into agitation, pressure, or spray techniques (Figure 1.25) [55]. Agitation methods use moist particles, bringing them into contact by mixing or tumbling so that the particle bonding forces can cause agglomeration. Pressure methods involve compaction or the extrusion of powders into small pellets. Spray techniques start either from suspensions, which are atomized into droplets and subsequently dried

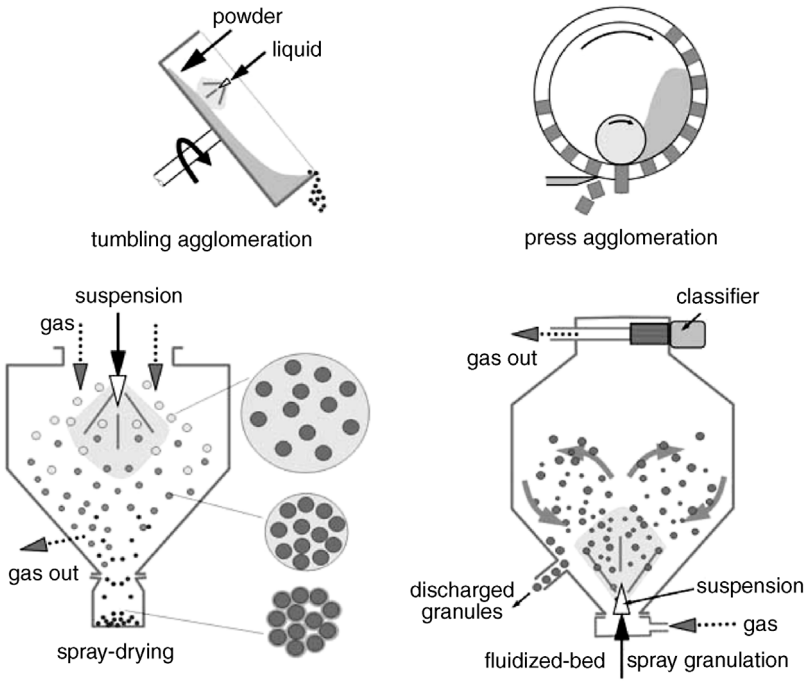

Figure 1.25 Common granulation methods (see text for details).

(spray-drying), or produce granules by spraying a liquid on a fluidized bed of powder particles (fluidized-bed spray granulation). Adhesion of the particles is mainly achieved by mobile liquids or binders. Mobile liquids cause capillary bonding forces, while binders form bridges among the particles. Granulation by agitation is carried out in either tumblers or mixers; agitation and pressure methods typically produce large granules, which are not suitable for dry pressing, but they can be used as feed material for calcining operations or injection molding. Granulates for ceramic dry pressing are commonly produced using spray methods.

1.5.1 Spray-Drying

Spray-drying is by far the most important granulation method. As most ceramic powders undergo a suspension-based pre-processing step such as wet milling or mixing, the combination of drying and agglomeration processes is obvious. Slurries used in such processes can be conditioned for further processing by adjusting the solid loading and dissolving the pressing aids in the suspension fluids. In spray-drying, the suspensions are atomized into small droplets and injected into a hot gas stream. In most cases, water is used as the suspension fluid and air as the drying gas, although in special cases organic liquids such as alcohol and inert drying gases are utilized. When in contact with the gas stream, the suspension fluid evaporates from the droplets. Ideally, the spherical shape of the droplets is preserved and the pressing aids are homogeneously precipitated onto the primary particle surfaces, after which the dry granules are separated from the gas stream and collected in a chamber. Atomization ideally results in the formation of droplets with the desired size and a narrow size distribution. It is carried out using centrifugal atomizers, pressure nozzles, or two-fluid nozzles [56–58]. The centrifugal atomizers use rotating disks or wheels to disintegrate the suspension; this low-pressure process results in mean droplet sizes of about 15–250 μm and a narrow droplet size distribution. Notably, the droplet size is decreased with the wheel speed and increased with the feed rate and viscosity. Other parameters that influence the droplet size include the surface tension and the solid loading. Two-fluid nozzles operate at moderate pressures for both the liquid and the atomization gas, with the particle size being controlled by the liquid : atomization gas ratio. In pressure nozzle atomization, the suspension is forced at high pressure through a nozzle orifice, where it is disintegrated into droplets. In this case the size distribution is narrower than for two-fluid nozzles, but wider than in rotational atomization; typically, the mean size increases with the feed rate and decreases with the pressure. Pressure nozzle atomizers form coarse particles of 120–300 μm, but require large drying chambers due to the high velocity of the spray.

Spray droplet and drying gas movement occur under cocurrent, countercurrent, or mixed-flow conditions. A cocurrent flow means flow in the same direction, and is applied to coarse products, whereas the countercurrent arrangement has excellent heat utilization and is applied to non-heat-sensitive materials. Both methods are integrated in the case of mixed-current flow, in which the drying chambers may have

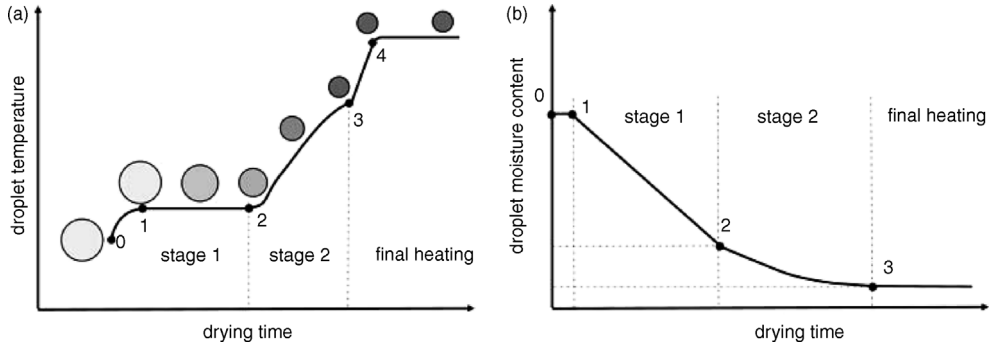

Figure 1.26 (a) Droplet temperature and (b) droplet moisture content during the characteristic stages of the spray-drying process. Modified from Ref. [59].

large dimensions of up to several meters, from the bottom of which the coarse granules can be discharged, with the chamber acting as a cyclone separator and the fines being separated by a second, high-efficiency cyclone separator.

Drying of the suspension droplets occurs in two characteristic stages [59] (Figure 1.26). The droplets reach equilibrium with the drying air within several milliseconds, without any significant change in moisture content; subsequently, the drying continues at a constant rate, as long as the surface remains saturated with the liquid. The droplet diameter decreases during this stage, but the surface temperature remains constant. At the so-called "critical point," the drying rate decreases, as the liquid–vapor interface recedes into the porous material and the subsurface temperature increases. This phase is extended until almost all of the liquid has evaporated. Ideally, the critical point is reached when the primary particles come into contact and form a homogeneous packing. A rapid drying and a high particle mobility favor the formation of a rigid particle shell at the surface, before the particles in the interior of the droplet come in contact with each other. In this case, the drying rate is decreased as the low permeability of the shell hinders the liquid flow to the surface. Ultimately, the shell structure leads to the formation of hollow granules that often exhibit craters or so-called "blow holes," formed by an inward collapse of the shell. Such collapse may be explained by the formation of a partial vacuum by the capillarity-induced movement of particles from the interior to the surface shell. Preferably, hollow granules should be avoided in ceramic pressing as they disturb the packing homogeneity and are clearly a source of pressing defects.

The characteristics of spray-dried granules depend on multiple parameters. Besides the drying conditions, the particles of the base powder and the additives introduced into the suspension play an important role. For example, to aid compaction the binders and plasticizers are usually added to the granules; however, the binders increase the viscosity of the suspensions and favor foaming, which in turn causes problems in the spray-drying process. Therefore, dispersants, and occasionally also defoaming agents, must be added to the slurries. Although, the interaction of these additives and the particle system during drying is very complex and no general

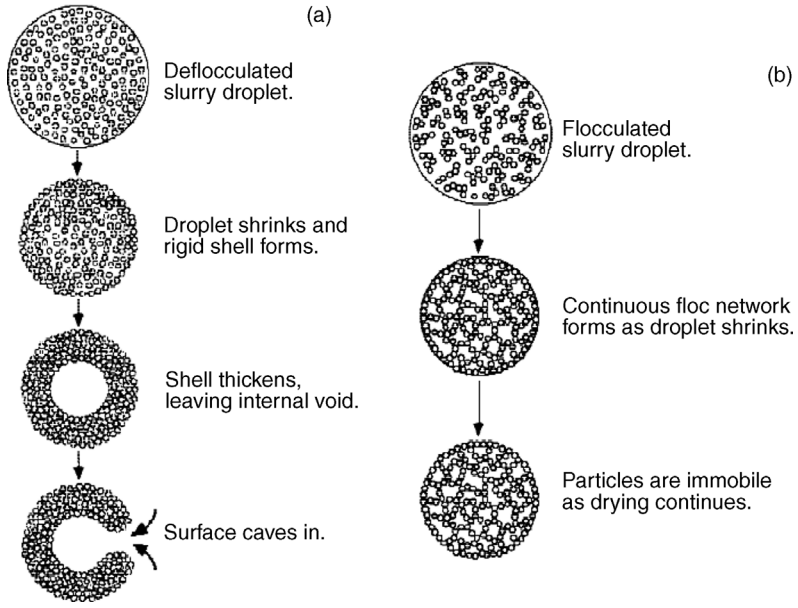

Figure 1.27 (a) Model of granule formation for deflocculated slurry; (b) Model of granule formation for flocculated slurry [60]. Reprinted by permission from American Ceramic Society; © 1999.

design rules exist, some basic findings were included in a model of granule formation by Walker and Reed [60] (see Figure 1.27).

As the ideal granule should be a uniform solid sphere, a too-rapid drying must be avoided as this causes the formation of a rigid surface, before the droplet has reached its stable spherical shape after atomization, and will result ultimately in a hollow granule. Hollow granules are favored by using highly deflocculated slurries and low solids loading of the suspension. Impressions of the structures of solid and hollow spray-dried granules, recorded using scanning electron microscopy, are shown in Figure 1.28.

A high solids loading and a certain degree of flocculation prevent shell formation and lead to the production of solid granules. The amount of dispersant used must be limited, as any overstabilization that enhances particle mobility will result in shell formation. Shear thinning behavior is favorable, in that low viscosities are required during the pumping and atomization of the slurries, which take place at high shear rates; however, high viscosities are required inside the drying droplet, where the shear rates tend towards zero. A certain slurry yield stress is needed to prevent shell formation, and this stress increases with the solid loading. The particle packing density inside the granules (outside the inner hole) is lower for the solid granules, and higher for the hollow granules. As droplet shrinkage during drying decreases with the solids loading, the mean granule size is larger for a higher solid loading of the slurries. These qualitative findings were confirmed for the spray-drying of practical granulates (e.g., Refs [61, 62]), and also in single-droplet model experiments [63, 64].

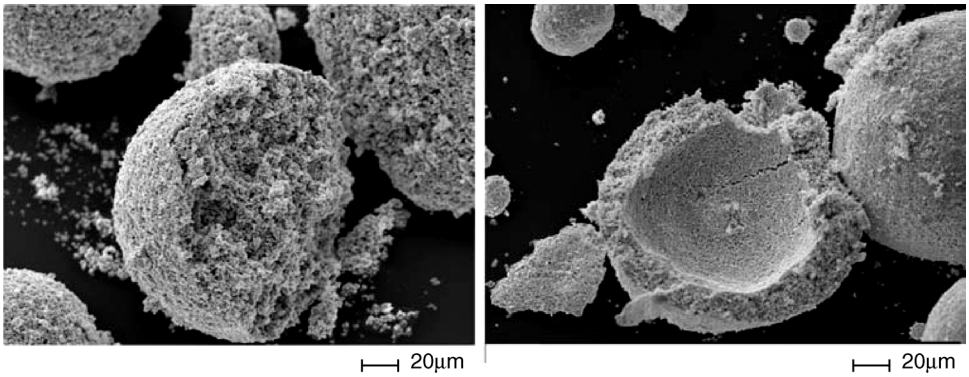

Figure 1.28 Solid and hollow spray-dried granules (granules were broken to demonstrate their structure).

As the slurry viscosity increases with decreasing particle size, powders with finer primary particles are sprayed from suspensions with lower solids loadings. Although a maximum solids loading of 50% has been reported for alumina particles with a mean diameter of 3 μm, as low as 26% solids loading was required for titania powder with 0.7 μm particles being sprayed from suspension [62].

1.5.2
Alternative Spray Granulation Methods

Spray-drying is also known in the form of freeze-spray-drying [65, 66], in which a water-based suspension is atomized and the droplets are sprayed into a container with liquid nitrogen, where they freeze instantaneously. Subsequently, the frozen granules are freeze-dried, which means that the liquid is sublimated. The packing structure remains unchanged during drying, which results in spherical and homogeneous granules with a loose packing of primary particles and low interparticle bonding forces. The granules are very soft and the binders are very homogeneously distributed. Although spray-freeze-drying remains a laboratory method, the unique properties of the granules make this method attractive for the controlled agglomeration of nanosized powders [67, 68]. Freeze-spray-dried nanostructured zirconia with 16 nm primary particles could be compacted to 50–55% of TD by dry pressing at 380 MPa, which was impossible to achieve with granulates prepared from the same powder by conventional spray-drying, even at higher pressures. Subsequent sintering to >98% of TD was achieved with the compacts having an average grain size of 70–80 nm, which was slightly higher than for the same powders consolidated by slip casting [68].

Fluidized-bed spray granulation [69] differs from conventional spray-drying in such a way that the atomized suspension droplets are deposited on the granule nuclei, which move around in a fluidized bed (Figure 1.25) where the drying energy is supplied by a hot gas. The repeated deposition of suspension droplets results in growth of the granules by layering agglomeration; those which have attained a given

size are then discharged from the fluidized bed. This technique results in spherical, dense and homogeneous granules with a narrow size distribution, for granules with sizes ranging from 100 μm up to several millimeters. This method has been applied to traditional ceramics [70], and also used to produce model granules from powders of technical ceramics [71].

1.5.3 Characterization of Ceramic Granulates

As noted above, multiple properties affect the further processing of ceramic granulates, the most important parameters being the granule size and shape distribution, the granule density, the fill and tap density, and the mass flow rate. More comprehensive characterization includes single granule strength and deformation measurements, residual moisture, and moisture sorption behavior.

The characterization of flow behavior during transport, storage and handling can be derived by using shear tests. Although these represent a common tool in bulk solid handling [72] (e.g., in silo design), the details of only a few shear tests on ceramic granulates have been reported [73, 74]. An example of the detailed characterization of ceramic granulates is provided in Ref. [73]. Details of the parameters acquired from such testing helps to understand and control the compaction behavior of the granulates and, ultimately, the properties of the compact and of the resultant sintered part.

References

1 Lange, F.F. (1989) Powder processing science and technology for increased reliability. *J. Am. Ceram. Soc.*, **72**, 3–15.
2 Reed, J.S. (1988) *Introduction to the Principles of Ceramic Processing*, Wiley-Interscience, New York.
3 Takahashi, M. and Suzuki, S. (1990) Compaction behaviour and mechanical characteristics of ceramic powders, in *Handbook of Ceramics and Composites*, vol. 1 (ed. N.P. Cheremisinoff), Marcel Dekker, Inc., New York and Basel, pp. 65–97.
4 McEntire., B.J. (1991) Dry pressing, in *Engineered Material Handbook*, vol. 4, *Ceramics and glasses* (ed. S.J. Schneider), ASM International, pp. 140–146.
5 Thümmler, F. and Oberacker., R. (1993) *Introduction to Powder Metallurgy*, The Institute of Materials, London.
6 German, R.M. (1994) Powder metallurgy science, in *Metal Powder Industries Federation*, 2nd edn, Princeton, New York.
7 Bortzmeyer, D. (1995) Dry pressing of ceramic powders, in *Ceramic Processing* (ed. R.A. Terpstra), Chapman & Hall, London, Weinheim.
8 Bortzmeyer, D. (1996) Die pressing and isostatic pressing, in *Processing of Ceramics* (ed. R.J. Brook), VCH Weinheim.
9 Rahaman., M.N. (2003) *Ceramic Processing and Sintering*, 2nd edn, Marcel Dekker, New York, Basel.
10 Beiss, P. (2010) Trends and innovations in powder compaction presses and die sets, in *International Powder Metallurgy Directory*, 14th edition. Inovar Communications Ltd, p. 29.
11 Schubert, H. (1984) Agglomerieren, in *Grundzüge der Verfahrenstechnik und Reaktionstechnik* (eds K. Dialer, U. Onken, and K. Leschonski), Carl Hanser Verlag München, Wien, p. 94.
12 Cumberland, D.J. and Crawford, R.J. (1987) The packing of particles, in

Handbook of Powder Technology, vol. 6, Elsevier, Amsterdam.
13 German, R.M. (1989) Particle packing characteristics, Metal Powder Industries Federation *(MPIF)*, Princeton, New York.
14 Wouterse, A. (2008) Random packing of granular matter. Ph.D. dissertation, University of Utrecht.
15 Aste, T., Saadatfar, M., and Senden, T.J. (2006) Local and global relations between the number of contacts and density in monodisperse sphere packs. *J. Stat. Mech.*, P07010.
16 Matheson, A.J. (1974) Computation of a random packing of hard spheres. *J. Phys. C Solid State*, **7**, 2569–2574.
17 Torquato, S., Trusquett, T.M., and Debenedetti, P.G. (2000) Is random close packing well defined? *Phys. Rev. Lett.*, **84**, 2064–2067.
18 Song, C., Wang, P., and Makse, H.A. (2008) A phase diagram for jammed matter. *Nature*, **453**, 629–632.
19 Kristiansen, K.deL., Wouterse, A., and Philipse., A. (2005) Simulation of random packing of binary sphere mixtures by mechanical contraction. *Physica – Section A*, **358**, 249–262.
20 Svarovsky, L. (1987) *Powder Testing Guide: Methods of Measuring the Physical Properties of Bulk Powders*, Elsevier Applied Science, London, New York.
21 (a) International Organization for Standardization (2008) ISO 4490: Metallic powders – Determination of flow rate by means of a calibrated funnel (Hall flowmeter); (b) International Organization for Standardization (2008) ISO 3923-1: Metallic powders – Determination of flow rate by means of a calibrated funnel (Hall flowmeter).
22 Arzt, E. and Fischmeister, H.F. (1979) Fundamental aspects of the compaction of metal powders. *Mem. Etud. Sci. Rev. Met.*, **76**, 573–579.
23 Helle, A.S. *et al.* (1985) Hot isostatic pressing diagrams. *Acta Metall. Mater.*, **33**, 2163–2174.
24 Fischmeister, H.F. and Arzt, E. (1982) Densification of powders by particle deformation. *Powder Metall.*, **26**, 82–88.
25 Schubert, J. (1998) Der Einfluss von Struktur und Verarbeitungseigenschaften keramischer Granulate auf die Werkstoffqualität. Ph.D. dissertation, TU Dresden.
26 Agniel, Y. (1993) Bedeutung der Einzelgranalieneigenschaften zur Defektvermeidung in trockengepressten keramischen Modellpulvern. Ph.D. dissertation, Universität Karlsruhe, 1992, Institute for Ceramics in Mechanical Engineering IKM 009.
27 Glass, S.J. and Ewsuk, K.G. (1997) Compaction science and technology. *MRS Bull.*, **22** (12), 24–28.
28 Lukasiewicz, S.J. and Reed, J.S. (1978) Character and compaction response of spray dried agglomerates. *Am. Ceram. Soc. Bull.*, **57**, 798–891.
29 Zheng, J. and Reed, J.S. (1988) Particle and granule parameters affecting compaction efficiency in dry pressing. *J. Am. Ceram. Soc.*, **71**, C456–C458.
30 Brewin, P.R., Coube, O., Doremus, P., and Tweed, J.H. (eds) (2007) *Modelling of Powder Die Compaction*, Springer, London.
31 Sinka, I.C. (2007) Modelling powder compaction. *Kona – Powder and Particle*, **25**, 4–22.
32 Harthong, B., Jérier, J.-F., Dorémus, P., Imbault, D., and Donzé, F.-V. (2009) Modeling of high-density compaction of granular materials by the discrete element method. *Int. J. Solids Struct.*, **46**, 3357–3364.
33 Skrinjar, O. and Larsson, P.-L. (2004) Cold compaction of composite powders with size ratio. *Acta Mater.*, **52**, 1871–1884.
34 Skrinjar, O. and Larsson, P.-L. (2004) On discrete element modelling of compaction of powders with size ratio. *Comp. Mater. Sci.*, **31**, 131–146.
35 Pizette, P., Martin, C.L., Delette, G., Sornay, P., and Sans, F. (2010) Compaction of aggregated ceramic powders: From contact laws to fracture and yield surfaces. *Powder Technol.*, **198**, 240–250.
36 Martin, C.L. and Bouvard, D. (2006) Discrete element simulation of the compaction of aggregated powders. *J. Am. Ceram. Soc.*, **89**, 3379–3387.
37 Balakrishnan, A., Pizette, P., Martin, C.L., Joshi, S.V., and Saha, B.P. (2010) Effect of particle size in aggregated and

agglomerated ceramic powders. *Acta Mater.*, **58**, 802–812.
38 Rumpf, H. (1970) Zur Theorie der Zugfestigkeit von Agglomeraten. *Chem.-Ing.-Tech.*, **42**, 538–540.
39 Bierwisch, C., Kraft, T., Riedel, H., and Moseler, M. (2009) Three-dimensional discrete element models for the granular statics and dynamics of powders in cavity filling. *J. Mech. Phys. Solids*, **57**, 10–31.
40 Bierwisch, C., Kraft, T., Riedel, H., and Moseler, M. (2009) Die filling optimization using three-dimensional discrete element modeling. *Powder Technol.*, **196**, 169–179.
41 Guo, Y., Kafui, K.D., Wu, C.-Y., Thornton, C., and Seville, J.P. (2009) A coupled DEM/CFD analysis of the effect of air on powder flow during die filling. *AICHE J.*, **55** (1), 49–62.
42 Cocks, A.C.F. (2007) Mechanics of powder compaction, in *Modelling of Powder Die Compaction* (eds P.R. Brewin, O. Coube, P. Doremus, and J.H. Tweed), Springer, London, pp. 31–43.
43 Sinka, I.C. and Cocks, A.C.F. (2007) Constitutive modelling of powder compaction – I. Theoretical concepts. *Mech. Mater.*, **39**, 392–403.
44 Sinka, I.C. and Cocks, A.C.F. (2007) Constitutive modelling of powder compaction – II. Evaluation of material data. *Mech. Mater.*, **39**, 404–416.
45 Shridar, I. and Fleck, N.A. (2000) Yield behaviour of cold compacted composite powders. *Acta Mater.*, **48**, 3341–3352.
46 Wikman, B., Bergman, G., Oldenburg, M., and Häggblad, H.-Å. (2006) Estimation of constitutive parameters for powder pressing by inverse modelling. *Struct. Multidisc. Optim.*, **31**, 400–409.
47 Xie, X. and Puri, V.M. (2006) Uniformity of powder die filling using a feed shoe: A review. *Particul. Sci. Technol.*, **24**, 411–426.
48 Wu, C.-Y., Dihoru, L., and Cocks, A.C.F. (2003) The flow of powder into simple and stepped dies. *Powder Technol.*, **134**, 24–39.
49 Schneider, L.C.R., Cocks, A.C.F., and Apostolopoulos, A. (2005) Comparison of filling behaviour of metallic, ceramic, hardmetal and magnetic powders. *Powder Metall.*, **48**, 77–84.
50 Product Brochures DORST Technologies (http://www.dorst.de); OSTERWALDER (http://www.osterwalder.com); LASCO (http://www.lasco.de); FETTE Compacting (http://www.fette-compacting.de); SMS MEER (http://www.sms-meer.com) (all accessed August 20, 2010).
51 Kennard, F. (1991) Cold isostatic pressing, in *Engineered Material Handbook*, vol. 4, *Ceramics and glasses* (ed. S.J. Schneider), ASM International, pp. 147–152.
52 Nishihara, M. and Koizumi, M. (eds) (1991) *Isostatic Pressing: Technology and Applications*, Springer, Netherlands, (New edition).
53 Höland, W., Schweiger, M., Rheinberger, V.M., and Kappert, H. (2009) Bioceramics and their application for dental restoration. *Adv. Appl. Ceram.*, **108**, 373–380.
54 Papen, E.L.J. (1977) Isostatic pressing, in *High Pressure Technology, Vol. II, Application and Processes* (eds I.L. Spain and J. Paauwe), Marcel Dekker, New York, pp. 339–389.
55 Lukasiewicz, S.J. (1991) Granulation and spray drying, in *Engineered Material Handbook*, vol. 4, *Ceramics and glasses* (ed. S.J. Schneider), ASM International, pp. 100–108.
56 Masters, K. (1991) *Spray Drying Handbook*, 5th edn, Longman Scientific Technical, Essex.
57 Masters, K. (1994) Applying spray drying to ceramics. *Am. Ceram. Soc. Bull.*, **73** (1), 63–72.
58 Celik, M. and Wendel, S.C. (2005) Spray drying and pharmaceutical applications, in *Handbook of Pharmaceutical Granulation Technology*, 2nd edn (ed. D.M. Parikh), Taylor & Francis, Boca Raton, pp. 129–157.
59 Mezhericher, M., Levy, A., and Borde, I. (2020) Theoretical models of single droplet drying kinetics: a review. *Dry. Technol.*, **28**, 278–293.
60 Walker, J. and Reed, J.S. (1999) Influence of slurry parameters on the characteristics of spray dried granules. *J. Am. Ceram. Soc.*, **82**, 1711–1719.

61 Tsetsekou, A., Agrafiotis, C., Leon, I., and Milias, A. (2001) Optimization of the rheological properties of alumina slurries for ceramic processing applications; part II: spray drying. *J. Eur. Ceram. Soc.*, **21**, 493–506.

62 Kim, D.-J. and Jung, J.-Y. (2007) Granule performance of zirconia/alumina composite powders spray-dried using polyvinyl pyrrolidone binder. *J. Eur. Ceram. Soc.*, **27**, 3177–3182.

63 Mahdjoub, H., Roy, P., Filiatre, C., Bertrand, G., and Coddet, C. (2005) Spray-dried ceramic powders: a quantitative correlation between slurry characteristics and shapes of the granules. *Chem. Eng. Sci.*, **60**, 95–102.

64 Bertrand, G., Roy, P., Filiatre, C., and Coddet, C. (2003) The effect of the slurry formulation upon the morphology of spray-dried yttria-stabilized zirconia particles. *J. Eur. Ceram. Soc.*, **23**, 1637–1648.

65 Uchida, N., Hiranami, T., Tanaka, S., and Uematsu, K. (2003) Spray-freeze-dried granules for ceramic fabrication. *Am. Ceram. Bull.*, **81** (2), 57–60.

66 Lyckfeldt, O., Rundgren, K., and Sjöstedt, M. (2004) Freeze granulation for the processing of silicon nitride ceramics. *Key Eng. Mater.*, **264–268**, 281–284.

67 Moritz, T. and Nagy, A. (2002) Preparation of super soft granules from nanosized ceramic powders by spray freezing. *J. Nano Res.*, **4**, 439–448.

68 Binner, J. and Vaidhyanathan, B. (2008) Processing of bulk nanostructured ceramics. *J. Eur. Ceram. Soc.*, **28**, 1329–1339.

69 Mörl, L., Heinrich, S., and Peglow, M. (2007) Fluidized bed spray granulation, in *Handbook of Powder Technology*, vol. 11, *Granulation* (ed. A.D. Salman), Elsevier, Amsterdam, pp. 21–188.

70 Rümpler, K. (1996) Thermal granulation of ceramic bodies in a fluidized bed. *cfi/Berichte der DKG*, **73**, 141–145.

71 Oberacker, R., Agniel, Y., and Thümmler, F. (1991) Relevance of single granule properties in compaction of granulated fine powders (in German), in *Pulvermetallurgie in Wissenschaft und Praxis*, vol. 7 (ed. H. Kolaska), VDI-Verlag, Düsseldorf, pp. 185–208.

72 Schwedes, J. (2003) Review on testers for measuring flow properties of bulk solids. *Granular Materials*, **5**, 1–43.

73 Nebelung, M. and Lang, B. (2009) Flowability of ceramic bulk materials. *CFI-Ceram. Forum. Int.*, **86** (3), E35–E40 and (4), E35–E38.

74 Freeman, R.E., Cooke, J.R., and Schneider, L.C.R. (2009) Measuring shear properties and normal stresses generated within a rotational shear cell for consolidated and non-consolidated powders. *Powder Technol.*, **190**, 65–69.